Continuous adjoint for Aerodynamic-Aeroacoustic optimization based on the Ffowcs Williams and Hawkings analogy

M. Monfaredi, X.S. Trompoukis, K.T. Tsiakas and K.C. Giannakoglou

National Technical University of Athens (NTUA), School of Mechanical Engineering,
Parallel CFD & Optimization Unit, Athens, Greece,
Morteza.monfaredi@gmail.com

Abstract. This paper presents an aerodynamic/aeroacoustic shape optimization framework, running on GPUs, based on the continuous adjoint method. The noise prediction tool and its adjoint are developed by implementing the Ffowcs Williams and Hawkings (FW-H) analogy, after integrating flow time-series, computed by an unsteady Euler equations solver, along a permeable surface. The accuracy of this hybrid solver is verified by comparing its outcome with that of a CFD run, for a 2D pitching airfoil in an inviscid flow. For the same case, the aeroacoustic noise and time-averaged lift gradients computed using the adjoint solver are verified w.r.t. finite differences. Finally, the adjoint solver is used to optimize the shape of the pitching airfoil, aiming at min. noise.

Keywords: Aerodynamics, Aeroacoustics, Shape Optimization, Continuous Adjoint, FW-H Analogy.

1 Introduction

Though adequately used in aerodynamic shape optimization, adjoint methods are relatively new in aeroacoustics. Among the few published works, a discrete adjoint to a hybrid URANS-FW-H solver, created using automatic differentiation, was developed to perform shape optimization for turbulent blunt trailing edge noise reduction [1], and far-field noise reduction for inviscid flow around a pitching airfoil [2]. In [3], the permeable FW-H formula in wave form is solved using a finite element method, leading to the necessary adjoint conditions at the interface between the Computational Fluid Dynamics (CFD) and Computational Aeroacoustics (CAA) domains. The continuous adjoint for a hybrid solver for incompressible flows using the Kirchhoff integral, for automotive applications can be found in [4]. This work, alongside with [6], expand the above to compressible flows by alternatively using the FW-H analogy. The verification of the method presented herein is restricted to the 2D unsteady inviscid flows.

2 The CFD/FW-H solver

The 2D unsteady inviscid flow equations of a compressible fluid are numerically solved in the CFD domain by the in-house GPU-enabled flow solver [5].

The Euler equations are discretized using a dual-time stepping method in which temporal derivatives are computed with second order accuracy. The spatial discretization is based on vertex-centered finite volumes, on unstructured grids. Convective fluxes are computed using the upwind Roe scheme with second order accuracy. The acoustic noise within the CAA domain is computed using the permeable version of the FW-H analogy. The pressure fluctuation in the frequency domain, at the receiver's location $\vec{x}_o$ can be written as [7]:

$$\hat{p}'(\vec{x}_o,\omega) = -\oint_{f=0} \hat{F}_i(\vec{x}_s,\omega)\frac{\partial \hat{G}(\vec{x}_o,\vec{x}_s,\omega)}{\partial x_{s_i}}ds - \oint_{f=0} i\omega\hat{Q}(\vec{x}_s,\omega)\hat{G}(\vec{x}_o,\vec{x}_s,\omega)ds \tag{1}$$

where $\hat{}$ represents the frequency domain variable and ω the frequency. The CFD and CAA domains overlap and f is the signed distance from their interface (FW-H surface) with positive f in the CAA domain, as shown in fig. 1(a). H is the Heaviside function and G is the 2D Green function for subsonic flows. $\vec{x}_s$ are the positions of the sources on the FW-H surface. Q and F_i are known as the monopole and dipole source terms respectively and are computed at the end of each time step during the flow solution. The quadrupole terms are neglected due to their small contribution. Details about the implementation of the FW-H solver can be found in [6].

3 The continuous adjoint method

The shape parameterization method employed utilizes Bezier polynomials, with control points denoted by b_i. For aeroacoustic problems, an objective function J, can be expressed by the following integral in the frequency domain:

$$J = \int_{\omega} \sqrt{\hat{p}'^2_{Re} + \hat{p}'^2_{Im}}\mathrm{d}\omega \tag{2}$$

where $\hat{p}'(\vec{x}_o,\omega)$ is the outcome of Eq. 1. Subscripts Re and Im refer to the real and imaginary parts of complex variables. In shape optimization, adjoint methods compute the gradient of J w.r.t. b_i. To formulate the continuous adjoint problem, an augmented objective function is defined as $F_{aug} = J + \int_T \int_\Omega \psi_n R_n d\Omega dt$, where $n = 1, 4$ and ψ_n, R_n, Ω and T are the adjoint variable fields, the residuals of the unsteady Euler equations, the CFD domain and the solution period, respectively. By differentiating F_{aug} w.r.t. b_i and setting the multipliers of the derivatives of the flow variables within the field integrals equal to zero, the unsteady adjoint equations are obtained:

$$-\frac{\partial \psi_m}{\partial t} - A_{nmk}\frac{\partial \psi_n}{\partial x_k} + S_{FW-H_m}\delta(f) = 0 \tag{3}$$

where $A_{nmk} = \frac{\delta f_{nk}}{\delta U_m}$, with U_m and f_{nk} being the conservative flow variables and inviscid fluxes, respectively. δ is the Dirac delta function and S_{FW-H_m} includes contributions from the FW-H analogy into the adjoint equations. This source term is added only along the FW-H surface. For the mathematical derivation

of this term one should refer to [6]. The expression that, finally, gives the J sensitivities is:

$$\frac{\delta J}{\delta b_i} = -\int_T \iint_\Omega \psi_n \frac{\partial U_n}{\partial x_k} \frac{\partial}{\partial t}\left(\frac{\delta x_k}{\delta b_i}\right) d\Omega dt - \int_T \iint_\Omega \psi_n \frac{\partial f_{nk}}{\partial x_e} \frac{\partial}{\partial x_k}\left(\frac{\delta x_e}{\delta b_i}\right) d\Omega dt - \int_T \iint_{S_w} \psi_n f_{nk} \frac{\delta n_k}{\delta b_i} ds dt \quad (4)$$

where n_k is the normal vector to the solid wall S_w. The workflow of an optimization loop is as follows: an unsteady flow solution is performed followed by the computation of the pressure fluctuations at the receiver's location using Eq. 1. Then, the adjoint solver computes S_{FW-H_m} and solves Eq. 3 by integrating it backwards in time. Upon completion of the adjoint solution, design sensitivities are computed using Eq. 4 and these are used to update b_i by means of a descent algorithm.

4 Verification of the hybrid CFD/FW-H solver

In order to verify the accuracy of the noise prediction method, results of the FW-H integral are compared to a well-known analytical solution of the sound field generated by a monopole source in a uniform flow. For the sake of shortness details are not included in this paper (see [1], [6]). Comparison of directivity plots in fig. 1(b), shows that the results of the FW-H integral exactly match the analytical solution. Next, the results of the CFD/FW-H are compared with the outcome of a pure unsteady CFD simulation. A NACA12 isolated airfoil is pitching about the quarter-chord point, in an inviscid flow with a 1 deg. amplitude and period equal to 0.114 sec with 40 time steps per period. The free-stream Mach number is $M_\infty = 0.4$. A 2D unstructured grid which extends 50 chords (chord length, C=1m) away from the airfoil is used, with 51000 nodes overall, among which 402 nodes on the airfoil contour and 151 nodes on the still FW-H surface at R=4C from the airfoil mid-chord (0.5C,0). The directivity pattern at R=20C is plotted in fig. 1(c) and shows a very good agreement between results of the unsteady CFD-based computation and the application of the FW-H integral on the flow time-series computed along the FW-H surface (hybrid solver).

5 Optimization results

Before proceeding to the aeroacoustic optimization, the gradients of the time-averaged lift and noise (Eq.2) computed by the adjoint method are verified w.r.t. finite differences (FD). The case and the grid is the same as the previous section, the only difference being that the Mach number and the amplitude of pitching are now equal to 0.6 and 2.4 deg, respectively. The airfoil pressure and suction sides are parameterized using two Bezier curves, with 8 control points which are free to move in the y direction. Since the first and last control points are fixed, this case has 12 design variables. Figure 2(a) and 2(b) show a good agreement with FD results for both of the time-averaged lift coefficient and noise, respectively.

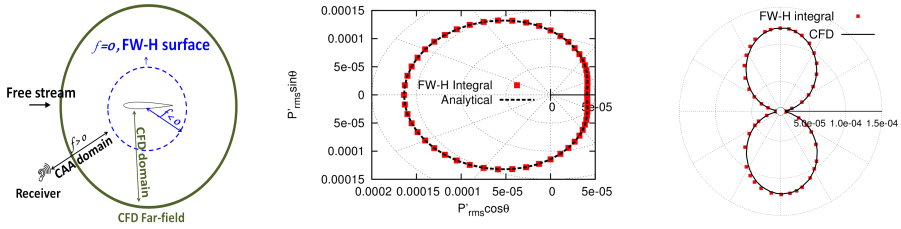

(a) (b) (c)

Fig. 1. (a) Sketch of the computational domain. (b) Monopole source in uniform flow with M = 0.6. Comparison of the directivity plots at R = 500m. (c) Directivity plot (p'_{rms}) around the pitching airfoil at radius R=20C.

Next, the optimization framework is used for aeroacoustic noise reduction. The receiver is located at $\vec{x}_o = (0, -20c)$. Three different sub-cases are considered. In Case 1, the whole airfoil shape can change during the optimization, while in Case 2 only the suction side can change. In Case 3, the shape of the trailing edge is fixed. As illustrated in fig.2(c), after 4 design cycles, the noise objective function, Eq. 2, is reduced by about 20%, 8% and 2%, in Cases 1, 2 and 3, respectively. In all cases, this results to a lower amplitude in pressure fluctuation in fig.2(d). Comparison of the sound directivity of the baseline and optimized airfoil of Case1 in fig.2(e) shows an omni-directional sound reduction. Figure 2(f) compares the baseline airfoil with the optimized shapes. It can be seen that the shapes optimized for noise are slightly thinner close to the leading edge and much thicker at the trailing edge (apart from Case 3 in which the trailing edge is fixed). The effect of the trailing edge as a main mechanism in noise generation can be seen by comparing Cases 2 and 3; keeping the trailing edge fixed during the optimization in Case 3 resulted in a lower drop in the noise objective value, even though a greater part of the airfoil is allowed to change. Regarding lift, the baseline airfoil has a zero lift coefficient due to its symmetrical shape and the pitching around the horizontal axis. The lift coefficient for the noise optimized shape in Case 1 becomes -0.89×10^{-3}. Freezing the shape of the pressure side in Case 2 and of the trailing edge in Case 3, increases the lift coefficient to 0.4345×10^{-2} and 0.415×10^{-3}, respectively.

6 Conclusions

The in-house flow/adjoint solver is extended to include an aeroacoustic noise prediction tool and its adjoint. Adjoint sensitivities are verified w.r.t. the FD for time averaged lift and noise. Aeroacoustic shape optimization is performed and results show that the objective function value is significantly improved; however, this considerably affect the aerodynamic performance. This highlights the importance of coupled aeroacoustic and aerodynamic optimization. Results of the aeroacoustic optimization in Case 3 showed the importance of the trailing edge shape in airfoil self noise generation.

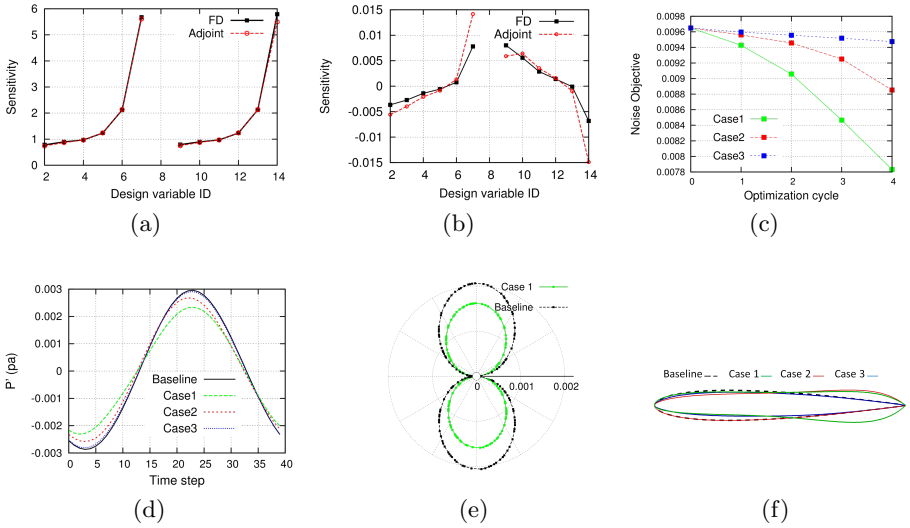

Fig. 2. (a) Time-averaged lift sensitivities using the adjoint method and FD. (b) Noise (Eq.2) sensitivities using the adjoint method and FD. (c) Value of objective function. (d)Time history of pressure fluctuation within a period. (e) Comparison of the directivity plot between the baseline and optimized airfoils after 4 design cycles. (f) Shape of the baseline and optimized airfoils after 4 design cycles.

7 Acknowledgments

This project has received funding from the European Union's Horizon 2020 research and innovation program under the Marie Skłodowska-Curie Grant Agreement No 722401.

References

1. Rumpfkeil, M., et al.: A hybrid algorithm for far-field noise minimization. Computers & Fluids 39(9), 1516–1528. 2010 doi:10.1016/j.compfluid.2010.05.006
2. Zhou, B., et al.: A discrete adjoint framework for unsteady aerodynamic and aeroacoustic optimization. AIAA Paper, 3355, 2015. doi:10.2514/6.2015-3355
3. Economon, T., et al.: A coupled-adjoint method for aerodynamic and aeroacoustic optimization. AIAA paper, 5598, 2012. doi:10.2514/6.2012-5598
4. Kapellos, C., et al. The unsteady continuous adjoint method for minimizing flow-induced sound radiation. Journal of Computational Physics 392: 368-384. 2019. doi:10.1016/j.jcp.2019.04.056
5. Kampolis, I., et al.: CFD-based analysis and two-level aerodynamic optimization on Graphics Processing Units. Computer Methods in Applied Mechanics and Engineering 199(9-12), 712-722. 2010 doi:10.1016/j.cma.2009.11.001
6. Monfaredi, M., et al. : An unsteady aerodynamic/aeroacoustic optimization framework using continuous adjoint. EUROGEN conf. Guimarães, Portugal, 2019
7. Lockard, D.: An efficient, two-dimensional implementation of the Ffowcs Williams and Hawkings equation. Journal of Sound and Vibration 229, no. 4 : 897-911. 2000 doi:10.1006/jsvi.1999.2522